PROJECT SQUID

TECHNICAL REPORT MIT-33-P

EXPERIMENTS ON A QUASI-STEADY J x B ACCELERATOR

By

R. LEON LEONARD AND JAMES A. FAY
MASSACHUSETTS INSTITUTE OF TECHNOLOGY

DEPARTMENT OF AEROSPACE ENGINEERING
SCHOOL OF ENGINEERING AND APPLIED SCIENCE
UNIVERSITY OF VIRGINIA
CHARLOTTESVILLE, VIRGINIA

Project SQUID is a cooperative program of basic research relating to Jet Propulsion. It is sponsored by the Office of Naval Research and is administered by the University of Virginia through Contract Nonr 3623(00), NR-098-038.

April 1964

Technical Report MIT-33-P

PROJECT SQUID

A COOPERATIVE PROGRAM OF FUNDAMENTAL RESEARCH
AS RELATED TO JET PROPULSION
OFFICE OF NAVAL RESEARCH, DEPARTMENT OF THE NAVY

Contract Nonr-3623(00), NR-098-038

EXPERIMENTS ON A QUASI-STEADY J x B ACCELERATOR*

by

R. Leon Leonard and James A. Fay
Massachusetts Institute of Technology
Cambridge, Massachusetts

April 1964

PROJECT SQUID HEADQUARTERS
DEPARTMENT OF AEROSPACE ENGINEERING
SCHOOL OF ENGINEERING AND APPLIED SCIENCE
UNIVERSITY OF VIRGINIA
CHARLOTTESVILLE, VIRGINIA

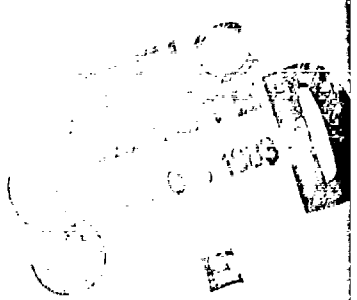

*Presented at the Fifth Symposium of Engineering Aspects of Magnetohydrodynamics, Cambridge, Massachusetts, 1-2 April 1964; and to be submitted for publication in the AIAA Journal.

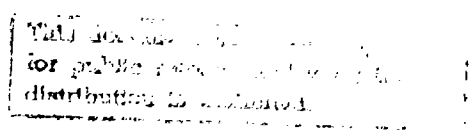

TABLE OF CONTENTS

Section		Page
	LIST OF ILLUSTRATIONS	v
	LIST OF SYMBOLS	vii
	ABSTRACT	ix
I.	INTRODUCTION	1
II.	EXPERIMENTAL APPARATUS AND METHODS OF MEASUREMENTS	4
III.	EXPERIMENTAL RESULTS	7
IV.	COMPARISON WITH THEORY	10
V.	CONCLUSION	15
	ACKNOWLEDGEMENT	16
	REFERENCES	17

LIST OF ILLUSTRATIONS

Fig. 1 Estimate of the value of $\omega\tau$ for the electrons and magnetic Reynolds number (R_{em}) as a function of electrode current (I) and applied magnetic field (B) for the accelerator at an initial pressure of 1 mm Hg. 21

Fig. 2 The x - t diagram for the shock tube and accelerator. 22

Fig. 3 A sketch of the accelerator section showing the field windings. . 23

Fig. 4 Current delivered through the electrodes for a typical run. 24

Fig. 5 A streak photograph of the flow in the accelerator. Curvature of the shock front, indicating acceleration of the gas can be observed. The streaks are due to gas particles of high luminosity. 25

Fig. 6 The potential difference between the electrodes for a typical run. During the period after the shock entered the electrodes and before the current was applied, the accelerator acted as a flowmeter. 26

Fig. 7 Calibration of the accelerator as a flowmeter. The flow velocity used in computing the ordinate was calculated from the measured shock velocity. 27

Fig. 8 Flow velocity as observed from streak photographs vs. shock front velocity. The line drawn was used to interpolate flow velocities for runs where streaks could not be distinguished, but in which the front velocity was measured. Straight line is the calculated particle velocity behind a shock whose velocity is given on the abscissa. 28

Fig. 9 The calculated induced voltage due to the accelerated gas in the magnetic field vs. the measured electrode potential showing the attainment of the E/B velocity. 29

Fig. 10 Momentum balance for the accelerator at an initial pressure of 1 mm Hg at various applied currents. The closed figures are interpolated values for Δu from Fig. 8. 30

Fig. 11 Momentum balance for the accelerator at an initial pressure of 1/2 mm Hg at various applied currents. The closed figures are interpolated values for Δu from Fig. 8. 31

Fig. 12 Momentum balance for the accelerator for various initial pressures. Data at 2 mm was taken from Hogan[20]. The closed figures are for Hogan's long accelerator and the open figures from his short accelerator; both are taken from his Fig. 15. . . . 32

Fig. 13 The velocity decrease at the exit of the accelerator. Straight line is the maximum theoretical decrease. 33

Fig. 14 Momentum balance for the accelerator assuming currents in the Hartmann boundary layer. The line drawn assumed losses predicted by an incompressible Hartmann profile assuming that the argon has transport properties equivalent to those of equilibrium argon at 1 atmosphere and 10,000°K. 34

List of Symbols

A	cross-sectional area of channel
B_0	applied magnetic field
B_1	magnetic field induced by j
d	channel width in direction of j or channel diameter
E	electric field
I	total current passed between electrodes
I_s	current short circuited through boundary layer
j	current density
J	boundary layer current per unit length
K	flowmeter calibration constant, Eq. (1)
ℓ^*	interaction length, $\rho u/\sigma B_0^2$
L	channel length
p	pressure
r	channel radius
u	axial flow velocity
V	electrode potential difference
x	axial distance
δ	Hartmann boundary layer thickness
Δp	pressure drop through accelerator
Δu	velocity increase in accelerator
Δu_e	velocity decrease at exit
ρ	gas density

σ electrical conductivity

μ viscosity

μ_0 vacuum magnetic permeability

$\omega\tau$ ratio of electron cyclotron frequency to collision frequency

Abstract

Experiments have been conducted on the acceleration of partially ionized argon in a channel of constant cross-sectional area having a uniform applied transverse magnetic field and subject to a current normal to both magnetic field and channel axis. The channel was operated in the manner of a shock tunnel with sufficient test time to achieve steady flow within the accelerator section. Visual observation of the flow within the channel and measurement of the electrical characteristics of the driving circuits established that substantial acceleration occurred in the channel. Measurements were made of the electrode potential and current and applied magnetic field. The maximum steady flow velocity within the magnetic field region, as measured from the streak photographs, was found to be approximately equal to the E/B velocity. Flow velocities up to 12 km/sec were thus measured. The increase in momentum of the gas within the accelerator was found to correlate with the theoretical impulse over the entire range tested. At the highest magnetic field strengths, a considerable decrease in velocity occurred as the gas left the magnetic field region at the downstream end of the accelerator. An estimate was made of the current flowing through a laminar Hartmann boundary layer on the tube wall normal to the magnetic field, and this calculated short circuit current was sufficient to account for the failure to achieve the theoretical momentum increase in the accelerator.

I. Introduction

The magnetic acceleration of a plasma in a steady, quasi-one-dimensional channel flow, accomplished by mutually perpendicular current, magnetic field, and flow velocity, has been the subject of many theoretical[1-8] and some experimental studies[9-14]. In particular, the theoretical studies have concentrated on the quasi-one-dimensional flow problem in which variation of magnetic induction (B, channel area (A) and electric field (E) or current density (j) were considered as variable functions of axial distance. In addition, theoretical studies of the effects of wall boundary layers and eddy current losses have also been undertaken[15-19]. On the experimental side, steady flow devices consisting of accelerators supplied by plasma arcs have shown that an increase in velocity can be achieved by this means[10-12]. A comparison of the results of these experiments with the previous theoretical studies is difficult to make, since there are considerable differences between the actual experimental configuration and the idealized models assumed in the theories. The shock tube experiments of Hogan[20], on the other hand, correspond more closely to the quasi-one-dimensional model of the theories, although they failed to provide a steady flow. In the experiments to be reported below, a steady flow of short duration has been achieved by shock tunnel techniques in a channel of uniform magnetic field, cross-sectional area, and electrode potential difference, thus extending the

experimental configuration of Hogan into the steady flow regime. For reasons to be explained below, it is believed that these experiments come reasonably close to duplicating the model assumed in the simple theories, and the results of the experiments have therefore been compared with such theories.

As explained in more detail below in section II, the accelerator channel of circular cross-section is supplied with partially ionized argon at about 12,000°K formed behind a shock wave reflected from the nearly-closed end of a larger diameter shock tube. The steadiness of the flow is assured by the critical flow into the accelerator channel of a volume of gas sufficient to fill the accelerator channel twice during the experiment. The constancy of electrode potential and magnetic field with axial distance along the accelerator is determined by the field winding and electrode construction. The effects of circular, as opposed to rectangular, cross-sectional shape are believed to be unimportant. On the other hand, Hall effects or relatively strong induced magnetic fields can cause appreciable departures from quasi-one-dimensionality. The possible importance of these effects have been investigated by estimating the value of $\omega\tau$ for the electrons and the magnetic Reynolds number based on tube radius for average gas conditions in the accelerator section. The estimates of these two dimensionless parameters are shown in Fig. 1 for the range of applied magnetic field strength and total current of the experiments, and it can be seen that

neither of them is large, which is sufficient reason to neglect Hall effects and induced fields in analyzing the results of the experiments.

The axial distance over which most of the acceleration takes place is the interaction length, $\ell^* = \rho u/\sigma B^2$ (see section IV below). The quasi-one-dimensional model assumes that this is greater than the tube radius, r. The ratio, ℓ^*/r, is also plotted in Fig. 1, from which it can be seen that two-dimensional effects may become important only at the highest magnetic field strengths.

The viscous Reynolds number of the flow, based upon tube diameter, is approximately 10^4. The boundary layers on the channel wall, either on the electrode or on the wall normal to the magnetic field (see section IV below), would be quite thin compared to the tube radius if the flow were laminar. (From the analysis given in section IV, it is concluded that the flow is laminar rather than turbulent.) As a consequence, the wall effects do not destroy the quasi-one-dimensional nature of the flow, and may be taken into account in the usual manner through boundary layer theory.

Having considered the principal aspects of the flow which determine how well it conforms to the simplified theories with which the measurements will be compared, we will proceed to discuss in greater detail the experimental apparatus and methods of measurement in section II, the results of the measurements in section III, and the interpretation of these measurements and comparison with the theories in section IV.

II. Experimental Apparatus and Methods of Measurement

These experiments were performed in a combustion-driven shock tube filled with argon at 1/2 or 1 mm Hg initial pressure. The 6 inch diameter, 20 foot long low-pressure section was joined to a 1.5 inch diameter extension by an end plate with rounded entrance but having no intervening diaphragm. Upon reflection of the Mach 11 incident shock wave from the end plate of the large diameter tube, a reservoir of stagnant argon at about 12,000°K and 1 or 2 atmospheres pressure is created, which thereupon flows into the smaller diameter tube. Initially a shock wave is propagated into the smaller tube (see wave diagram of Fig. 2), followed by a small expansion wave which brings the flow at the entrance to a steady state. There are thus two contact interfaces in the small tube. The first is caused by a temperature difference between the gas initially in the small tube and its driver gas (originally the test gas in the 6" tube). The second interface is between the argon and the combustion products of the original driver gas. The temperature difference across the first contact interface was calculated to be quite small, thus giving a reasonably homogeneous flow of test gas at a velocity of 3000 m/sec.

The accelerator section of the smaller tube (Fig. 3), made from Grade #950 Panalyte tubing of 1.5 inch I.D. with a 1/2 inch wall thickness, was located 3 feet from the end plate. The electrodes were made from .065 inch thick copper strip, 24 inches long and subtending an angle

of 60° in the circumferential direction. A longitudinal slit was cut in the accelerator wall half way between the two electrodes and closed with a plexiglass window. This window permitted observation of the flow using a rotating mirror camera.

Current was supplied to the electrodes by a lumped parameter transmission line capacitor bank with six sections, each of which had a 400 μf capacitor and a 1 μh inductor. The impedance of the leads used was large compared to that of the electrode gap, and hence a nearly constant current was obtained. Current variations with time were due to imperfect components in the transmission line rather than variations in the gas impedance. A typical current discharge is shown in Fig. 4. The current was initiated when the shock was 3" inside the electrodes and returned to zero at approximately the same time the second contact interface left the electrodes. The maximum current obtained from this source was 16,000 amps.

A 14 turn air-core coil was used to generate an applied transverse magnetic field. The coil was saddle-shaped around the accelerator section as shown in Fig. 3, thus minimizing the volume in which magnetic energy was stored. The coil was made from #5 insulated copper wire and was connected in series with a 4600 μf capacitor bank. The circuit was closed with an ignitron when the shock wave was far upstream so as to permit the field to reach a peak value when the drive current was applied. The circuit rang with a half cycle time of 2.05 milliseconds permitting

negligible variations in field strength over the 250 μs time of the experiment. The maximum field strength obtained was 9000 gauss.

The orientation and polarity of the leads supplying the electrodes were such that the magnetic induction caused by this current added to the applied magnetic field. This was accomplished by supplying the current at the upstream end of the electrodes.

For each run, the following quantities were measured:

(1) Shock and flow velocities. The shock front velocity was measured in the 6" section and in the 1 1/2" section upstream of the accelerator using ionization probes. A rotating mirror camera streak photograph was taken of the slit in the side of the accelerator channel (Fig. 5), from which it was possible to determine the front velocity from the slope of the front on the photograph. Similarly, luminosity streaks seen in the flow behind the shock front were assumed to move with the gas bulk velocity, and their speed was determined in the same manner as that of the shock front, thus giving a flow velocity for the gas. The camera could be directed at any part of the flow channel, and photographs were taken both of the flow in the accelerator and downstream of the accelerator.

(2) Electrical conductivity. The electrical conductivity (σ) of the test gas was measured upstream of the accelerator by the method described by Lin, Kesler and Kantrowitz[22]. The upstream conductivity decreased gradually during the test time, and had an average value of 15 mho/cm.

(3) Applied current through the electrodes. The total current flowing between the electrodes was measured using a current transformer. The output of this transformer was integrated and displayed on an oscilloscope (Fig. 4). During operation of the accelerator, no variation in current with either magnetic field strength or gas density was observed.

(4) Magnetic field strength. The strength of the magnetic field for each run was determined by measuring the current flowing in the L-C circuit composed of the field coil and the capacitor bank. This current was then related to the magnetic field strength using a search coil calibration. The results of the search coil calibration were checked with a theoretical calculation of the field expected for a given current.

(5) Electrode potential. The potential difference between the electrodes in the accelerator was measured at the downstream end of the electrodes (see Fig. 6). To determine whether the electrodes were equipotential surfaces, a measurement of potential was also made at the upstream end of the electrodes which agreed with downstream measurements to within the experimental error.

III. Experimental Results

Before the acceleration experiment was started by initiating the electrode current pulse, there was a short time (on the order of 25 μs) when the shock wave partially covered the electrodes and hence a voltage (V) was induced across the electrodes by the gas flow perpendicular to the magnetic field. Measurements of this induced voltage

were made for every run and are shown in Fig. 7 plotted as a function of the product of flow velocity, magnetic field strength and tube diameter. The velocity used was the equilibrium flow velocity behind a shock of strength measured just upstream of the accelerator. The magnetic field strength used was the value taken just before the drive current was applied. The line drawn which fitted the data best can be taken as a calibration curve for the accelerator operating as a flowmeter.

Fishman[23] made an analytical study of the linear MHD accelerator of circular cross-section in which he assumed the magnetic Reynolds number and interaction parameter based on the channel diameter (d) were both small compared with unity and that the conductivity was a scalar. He found that for the electrode configuration of this experiment the calibration constant, defined by

$$K \equiv V/duB_0 \qquad (1)$$

was 0.91. This compares quite favorably with Fig. 7 for which K = 5/6.

Measurements of the maximum shock front velocity and maximum gas flow velocity in the accelerator were made from streak photographs like that shown in Fig. 6. For all the test runs, a measurement of shock front velocity was made; and for more than half the runs it was possible to distinguish streaks from which a flow velocity could be obtained. In order to interpolate for values of flow velocity for those runs where no

streak measurement could be made, Fig. 8 was prepared from the remaining runs (for which both front and flow velocities could be measured), and an average line was drawn. This line was taken as the correlation between flow and front velocities when only the latter was measured, and results based on this method of interpolation were used in subsequent analysis of the data.

In Fig. 6, the line labeled "real gas flow velocity" is the calculated value for the particle behind a shock wave of strength indicated on the abscissa. It was expected that far behind the incident shock, in the steady flow region, the flow velocity need not correspond to the equilibrium velocity behind the initial shock wave, and this seems clearly to be the case.

If the interaction length, ℓ^*, is small compared to the electrode length, the gas should attain the E/B_0 velocity close to the upstream end of the electrodes, and hence no current will flow near the downstream end. If the measured electrode potential is equal to $KduB_0$, where u is the maximum flow velocity in the accelerator, then the E/B_0 velocity must have been attained. In Fig. 9 is plotted the electrode potential as a function of duB, using as data the average measured electrode potential over the duration of current flow, the average imposed magnetic field during that time, and the maximum observed (or interpolated) flow velocity for the run. It can be seen that a line of slope $K = 5/6$ correlates the data fairly well.

When ℓ^* is comparable with, or greater than the electrode length, the electrode potential will be greater than $KduB_0$. This can be seen to be the case in Fig. 9, for the electrode potential exceeds this value when uB is small, and hence ℓ^* is large.

IV. Comparison with Theory

For a steady quasi-one-dimensional flow in a rectangular channel of constant area A, constant applied magnetic induction B_0, and constant electric field E, the equations of momentum and magnetic induction, and scalar Ohm's law, are:

$$\rho u \frac{du}{dx} = - \frac{dp}{dx} + j(B_0 + B_1) \tag{2}$$

$$\mu_0 j = - \frac{dB_1}{dx} \tag{3}$$

$$j = \sigma[E - u(B_0 + B_1)] \tag{4}$$

in which the current density j is assumed uniform over the cross section, the magnetic induction B_1 due to j is assumed to add to B_0, σ is the scalar electrical conductivity and ρu is the constant mass flow per unit area. For a channel of rectangular cross section of area A and width d in the direction of j, Eqs. (2) and (3) may be integrated over the volume of the accelerator, resulting in:

$$\Delta u = \frac{1}{\rho u} \left\{ \Delta p + \frac{\mu_0}{2} \left(\frac{Id}{A}\right)^2 + \frac{B_0 \, Id}{A} \right\} \tag{5}$$

in which Δu is the increase in velocity of the fluid, Δp is the decrease in static pressure in the direction of flow and $\mu_0 I^2 d^2/2A^2$ is the "back-strap" effect of the total applied current I which adds to the total magnetic induction.

For a channel of circular cross section of diameter d, we use $A = \pi d^2/4$ in Eq. (5), which gives the correct volume integral of jB_0, and a reasonable estimate for that of jB_1.

The values of Δu measured from the streak photographs or interpolated from the front velocity measurements as shown in Fig. 8, are plotted in Figs. 10 and 11 as a function of the theoretical velocity increase calculated from the right hand side of Eq. (5). In calculating the theoretical Δu, the mass flux ρu was calculated for the critical flow from the stagnation conditions behind the reflected shock wave and Δp was assumed to equal the static pressure for this critical flow, i.e., the downstream pressure was assumed negligible. I and B_0 were measured for each experiment.

From Figs. 10 and 11 it can be seen that the measured velocity increase lies between 50% and 100% of the theoretical value, the former ratio applying at the higher accelerations. If we denote the ratio of actual to theoretical velocity increase by the term momentum efficiency (η), then the momentum efficiency depends mostly upon the theoretical velocity increase and not upon the gas density, as can be seen from Fig. 12 which summarizes the results of our experiments and those of Hogan[20],

all of which cover a fourfold variation of gas density. Furthermore, a careful examination of Figs. 10 and 11 shows that there is no distinction in performance between equal accelerations produced by large I and small B_0 or vice versa.

For the larger values of Δu, the dominant term on the right hand side of Eq. (5) is the last. The first term varied from 90% to 25% of the whole, while the second term varied between 15% and 7%, over the range of low to high accelerations. The larger percent scatter of the points at low Δu are probably due to the uncertainty in the first two terms as well as to the inaccuracy in the measurement of Δu. The overall accuracy of the experimental points is about $\pm$ 20%.

The variation of velocity with distance along the channel may be estimated from Eqs. (2) - (4) under the assumptions that $B_1 << B_0$ and that p and σ are constant, with the result that Eq. (2) integrates to:

$$u = u_i + \Delta u \{1 - e^{-x/\ell^*}\}/\{1 - e^{-L/\ell^*}\} \qquad (6)$$

where

$$\ell^* \equiv \rho u/\sigma B_0^2 \qquad (7)$$

and in which u_i is the initial velocity and L is the accelerator length. The length ℓ^* was not measured from the streak photographs, but it could be seen qualitatively that the acceleration occurred in a shorter distance at the higher values of B_0.

As mentioned in section III, considerable deceleration of the flow occurred at the exit of the accelerator where B_0 decreased to zero in about one tube diameter. This deceleration was measured in only a few instances under conditions of maximum B_0. This decrease in velocity Δu_e would not be expected to exceed that due to a sudden decrease in magnetic pressure of amount $B_0^2/2\mu_0$:

$$\rho u \, \Delta u_e \leq B_0^2/2\mu_0 \tag{8}$$

this latter being the limiting value of Δu_e at high magnetic Reynolds number. The few measurements of Δu_e are plotted in Fig. 13 as a function of $B_0^2/2\mu_0 \, \rho u$, from which it can be seen that this inequality is approximately satisfied. This deceleration could be considerably reduced by gradually reducing B_0 over many tube diameters, thereby decreasing the magnitude of the eddy currents which brake the flow.

The failure of the flow to accelerate to the theoretical value is most likely due to the leakage of current between the electrodes through the boundary layer which forms on the sides of the tube normal to B_0. In this Hartmann boundary layer the viscous stress is balanced by the Lorentz force, so that the boundary layer grows, in a distance ℓ^* from the beginning of the electrode, to a characteristic thickness δ:[18]

$$\delta = (\mu/\sigma B_0^2)^{1/2} \tag{9}$$

and thereafter remains constant in thickness. The total current J flowing through this boundary layer per unit axial length is[15]

$$J = \sigma u B_0 \delta \tag{10}$$

provided σ and the viscosity μ are constant, and the free stream velocity u is equal to F/B_0, which is achieved in the accelerator for $x > \ell^*$. Assuming that ℓ^* is much less than the length of the electrodes L, the total leakage current I_s through the two boundary layers on each side of the tube is:

$$I_s = 2(u_i + \Delta u)\,(\mu\sigma)^{1/2}\, L \tag{11}$$

by virtue of Eqs. (9) and (10).

There is no way to measure this leakage current directly. However, if this current is sufficient to account for the failure to achieve the theoretical momentum increase, then Eq. (5) ought to be satisfied if I is replaced by the actual total current to flow through the inviscid core, namely $1 - I_s$. Inserting this latter value only in the last term on the right hand side of Eq. (4)[+], and making use of Eq. (11), the modified momentum balance may be written as:

$$\frac{\Delta p + \frac{\mu_0}{2}\left(\frac{Id}{A}\right)^2 + \frac{IB_0 d}{A} + \rho u\, u_i}{\rho u(u_i + \Delta u)} = 1 + \frac{2(\mu\sigma)^{1/2}\, L\, dB_0}{\rho u A} \tag{12}$$

[+] Because the middle term is considerably smaller than the others, it was not deemed necessary to correct it for the leakage current.

In Fig. 14 the left hand side of Eq. (12), as computed for the measured and estimated quantities contained therein, is plotted as a function of $B_0/\rho u A$. A straight line of slope $2(\mu\sigma)^{1/2}$ Ld is also drawn, using values of σ = 3,000 mhos/m and $\mu = 3 \times 10^{-4}$ Kgm/m sec, which are appropriate for argon[24] at 10,000°K. Although the scatter is large, the major effect of the current leakage through the laminar Hartmann layer, as depicted in Eq. (12), is borne out by the experimental measurements, and the dependence upon the principal parameters is generally as described therein.

The calculations outlined above assume that the boundary layer is laminar. Using the values of σ and μ quoted above, the viscous Reynolds number based on the Hartmann layer thickness (or the ratio of Reynolds to Hartmann number) is about 140 under test conditions giving maximum Δu. For liquid metal flows, this is sufficient to ensure laminar flow.

If the boundary layer were turbulent, then it is to be expected that I would also depend upon B_0 and the right hand side of Eq. (12) would not be linear in B. The data of Fig. 14 are not sufficiently accurate to determine conclusively whether this dependence is not linear.

V. Conclusions

1. Operating under conditions for which a quasi-one-dimensional flow analysis should be applicable, the velocity increment in the accelerator was found to correlate with the theoretical value given by the simple theory over a wide range of gas densities, magnetic field strengths, and total current.

2. A laminar Hartmann boundary layer analysis showed that the expected leakage current could account quantitatively for the failure to achieve the theoretical velocity increase as predicted by the simple theory.

3. The considerable plasma deceleration at the exit of the accelerator could be quantitatively related to the sudden decrease in the applied magnetic field.

Acknowledgment

This research was supported by Project Squid through the Office of Naval Research under Contract Nonr 3623(S2). The authors are indebted to F. Fraim and P. Croce for their invaluable aid in conducting the experiments.

References

1. Resler, E. L. and Sears, W. R., "The prospects for magnetoaerodynamics," J. Aero/Space Sci. 25, 235-245 (1958).
2. Resler, E. L., and Sears, W. R., "Magnetogasdynamic channel flow," ZAMP IXb, 509-518 (1958).
3. Wood, G. P. and Carter, A. F., "Considerations in the design of a steady-flow dc plasma accelerator" in Dynamics of Conducting Gases, ed. by A. B. Cambel and J. R. Fenn (Northwestern University Press, Evanston, Illinois, 1960) pp. 201-212.
4. Kerrebrock, J. L. and Marble, F. E., "Constant-temperature magnetogasdynamic channel flow," J. Aero/Space Sci. 27, 78 (1960).
5. Podolsky, B. and Borman, G., "The electromagnetic acceleration of a continuously flowing plasma," in Plasma Acceleration, ed. by S. Kash (Stanford University Press, Stanford, Calif., 1960) pp. 12-29.
6. Oates, G. C., Richmond, J. K., Aoki, Y. and Grohs, G., "Loss mechanisms of a low temperature plasma" in Magnetohydrodynamics, ed. by A. B. Cambel, T. P. Anderson and M. M. Slawsky (Northwestern University Press, Evanston, Illinois, 1962) pp. 207-230.
7. Sherman, H., "Theoretical performance of a crossed field MHD accelerator," ARS Journal 32, 414-420 (1962).
8. Drake, J. H., "Optimum isothermal acceleration of a plasma with constant magnetic field," AIAA Journal 1, 2053-2057 (1963).
9. Wood, G. P., Carter, A. F., Sabol, A. P., and Weinstein, R. H., "Experiments in steady state crossed-field acceleration of plasma," Phys. Fluids 4, 652-653 (1961).

10. Demetriades, S. T. and Ziemer, R. W., "Energy transfer to plasmas by continuous Lorentz forces," in Magnetohydrodynamics, ed. by A. B. Cambel, T. P. Anderson and M. M. Slawsky (Northwestern University Press, Evanston, Illinois, 1962) pp. 185-205.

11. Demetriades, S. T., "Experimental magnetogasdynamic engine for argon, nitrogen and air," in Proceedings of the Second Symposium on the Engineering Aspects of Magnetohydrodynamics," ed. by C. Mannal and N. W. Mather (Columbia University Press, New York, 1962) pp. 19-44.

12. Carter, A. F., Wood, G. P., Sabol, A. P. and Weinstein, R. H., "Experiments in steady-state high-density plasma acceleration," in Proceedings of the Second Symposium on the Engineering Aspects of Magnetohydrodynamics, ed. by C. Mannal and N. W. Mather (Columbia University Press, New York, 1962) pp. 45-55.

13. Ragusa, D. and Baker, J., "Experimental results with a direct current electromagnetic plasma accelerator," in Proceedings of the Second Symposium on the Engineering Aspects of Magnetohydrodynamics," ed. by C. Mannal and N. W. Mather (Columbia University Press, New York, 1962) pp. 56-63.

14. Demetriades, S. T., and Lenn, P. D., "Electrical discharge across a supersonic jet of plasma in transverse magnetic field," AIAA Journal 1, 234-236 (1963).

15. Fay, J. A., "Hall effects in a laminar boundary layer of the Hartmann type," Research Report 81, AFOSR TN 60-291 (Avco-Everett Research Laboratory, Everett, Mass., 1959).

16. Kerrebrock, J. L., "Similar solutions for boundary layers in constant-temperature magneto-gasdynamic channel flow," J. Aero/Space Sci. 27, 156-157 (1960).

17. Kerrebrock, J. L., "Electrode boundary layers in direct-current plasma accelerators," J. Aero/Space Sci. 28, 631-643 (1961).

18. Fay, J. A., "Plasma boundary layers" in Magnetohydrodynamics, ed. by A. B. Cambel, T. P. Anderson and M. M. Slawsky (Northwestern University Press, Evanston, Illinois, 1962) pp. 337-348.

19. Culick, F. E., "A boundary-layer problem associated with magnetogas-dynamic channel flow," AIAA Journal 1, 2666-2668 (1963).

20. Hogan, W., "An experimental investigation of a magnetogasdynamic accelerator," in Proceedings of the Third Symposium on the Engineering Aspects of Magnetohydrodynamics (to be published. Also published as Magnetogasdynamics Laboratory Report No. 62-1, Dept. of Mechanical Engineering, Massachusetts Institute of Technology, Cambridge, Mass., 1962).

21. Arave, R. J. and Hurly, O. A., "Aerothermodynamic Properties of High Temperature Argon," Document D2-11238, (Boeing Aircraft Co., Seattle, Wash., 1962).

22. Lin, S. C., Resler, E. L. and Kantrowitz, A., "Electrical conductivity of highly ionized argon produced by shock waves," J. App. Phys. 26, 95-109 (1955).

23. Fishmann, F., "Steady magnetohydrodynamic flow through a channel of circular section," Research Report No. 97, (Avco-Everett Research Lab., Everett, Mass., 1960).

24. Amdur, I., and Mason, E. A., "Properties of gases at very high temperatures," Phys. Fluids 1, 370-383 (1958).

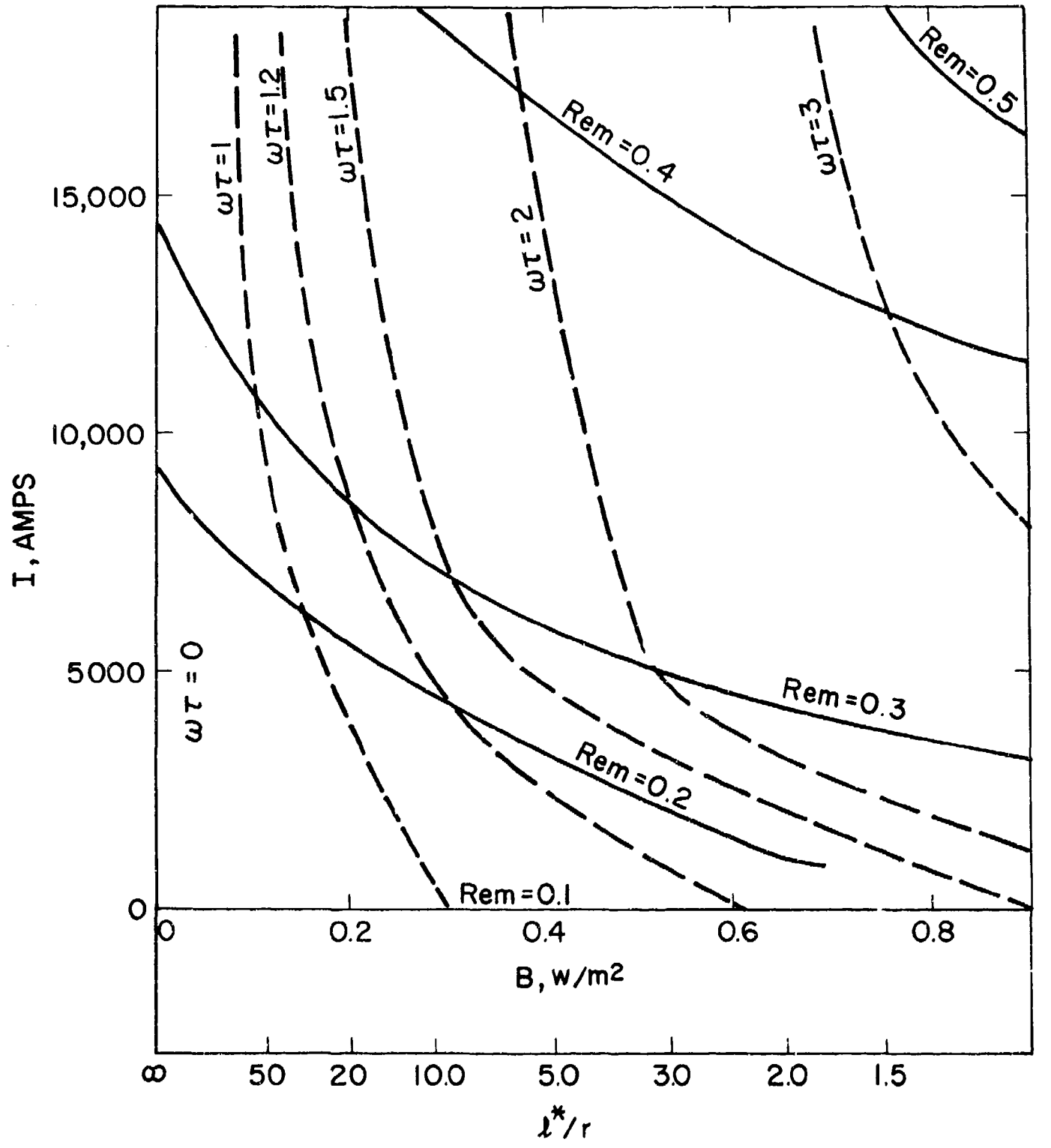

Fig. 1 Estimate of the value of $\omega\tau$ for the electrons and magnetic Reynolds number (R_{em}) as a function of electrode current (I) and applied magnetic field (B) for the accelerator at an initial pressure of 1 mm Hg.

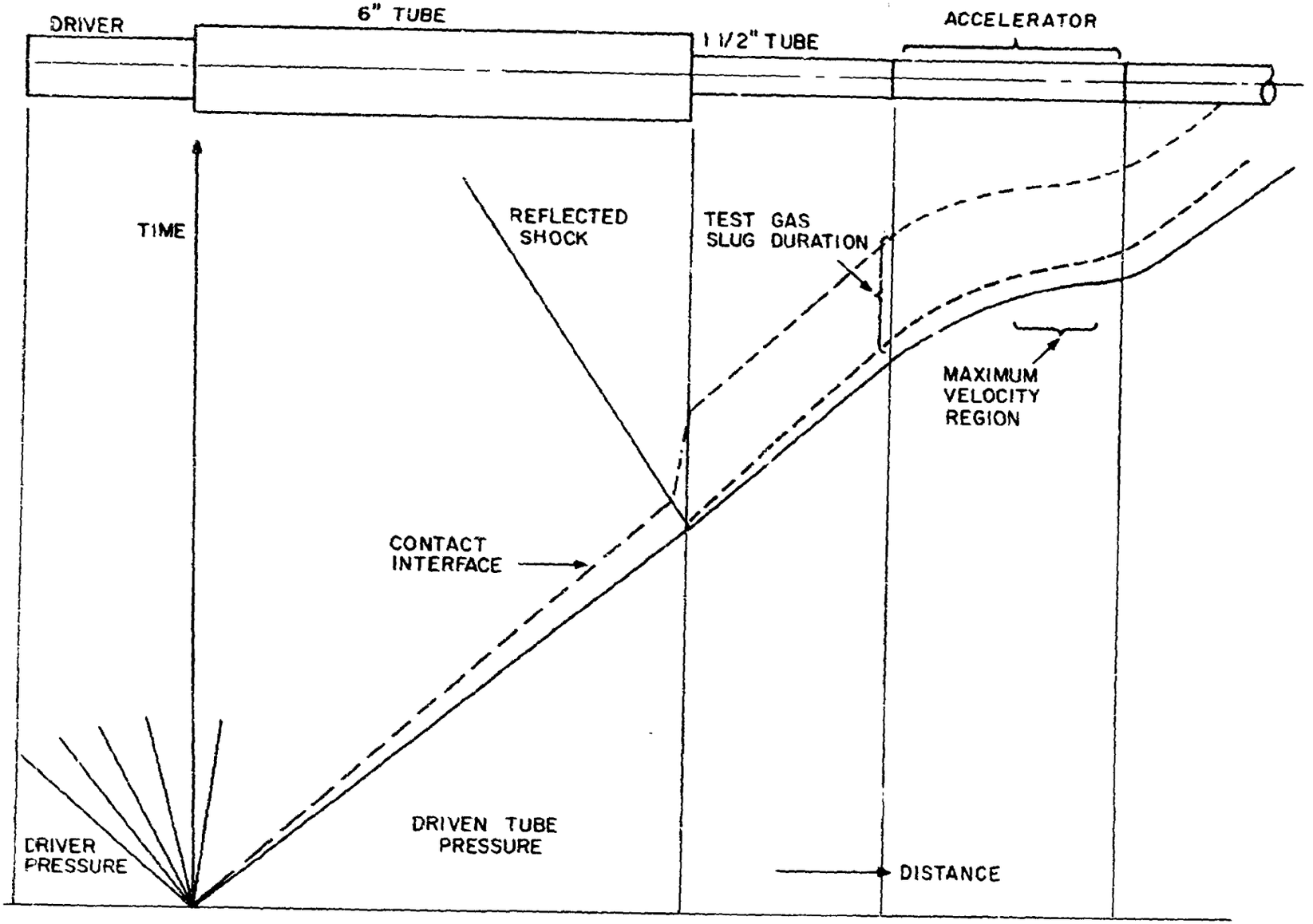

Fig. 2 The x - t diagram for the shock tube and accelerator.

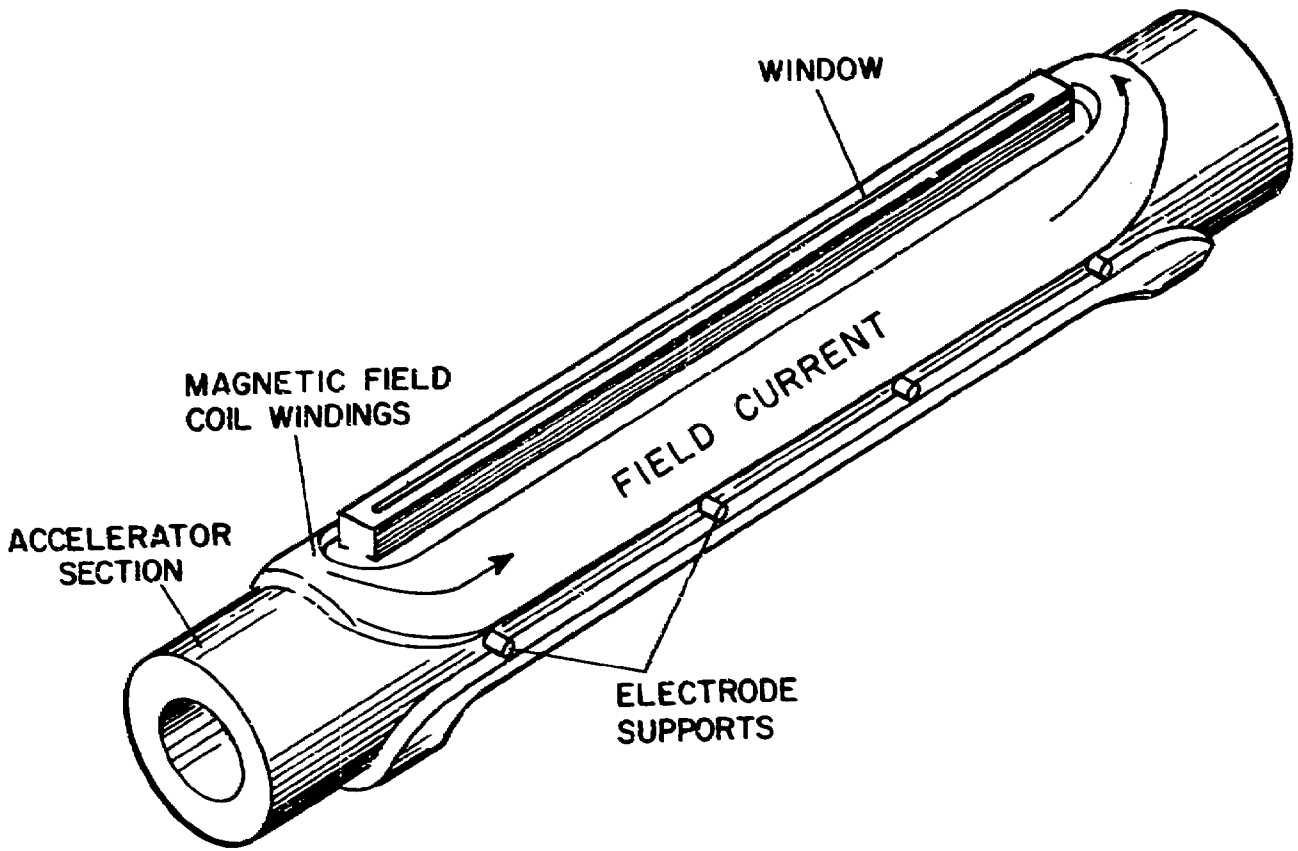

Fig. 3 A sketch of the accelerator section showing the field windings.

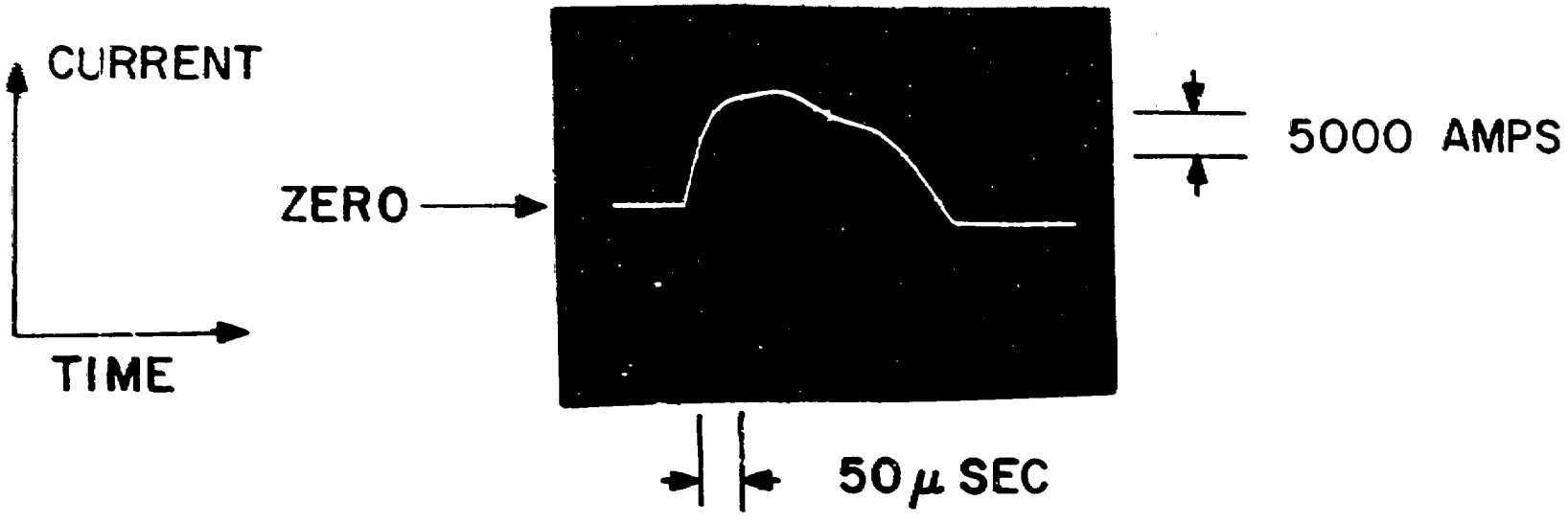

Fig. 4 Current delivered through the electrodes for a typical run.

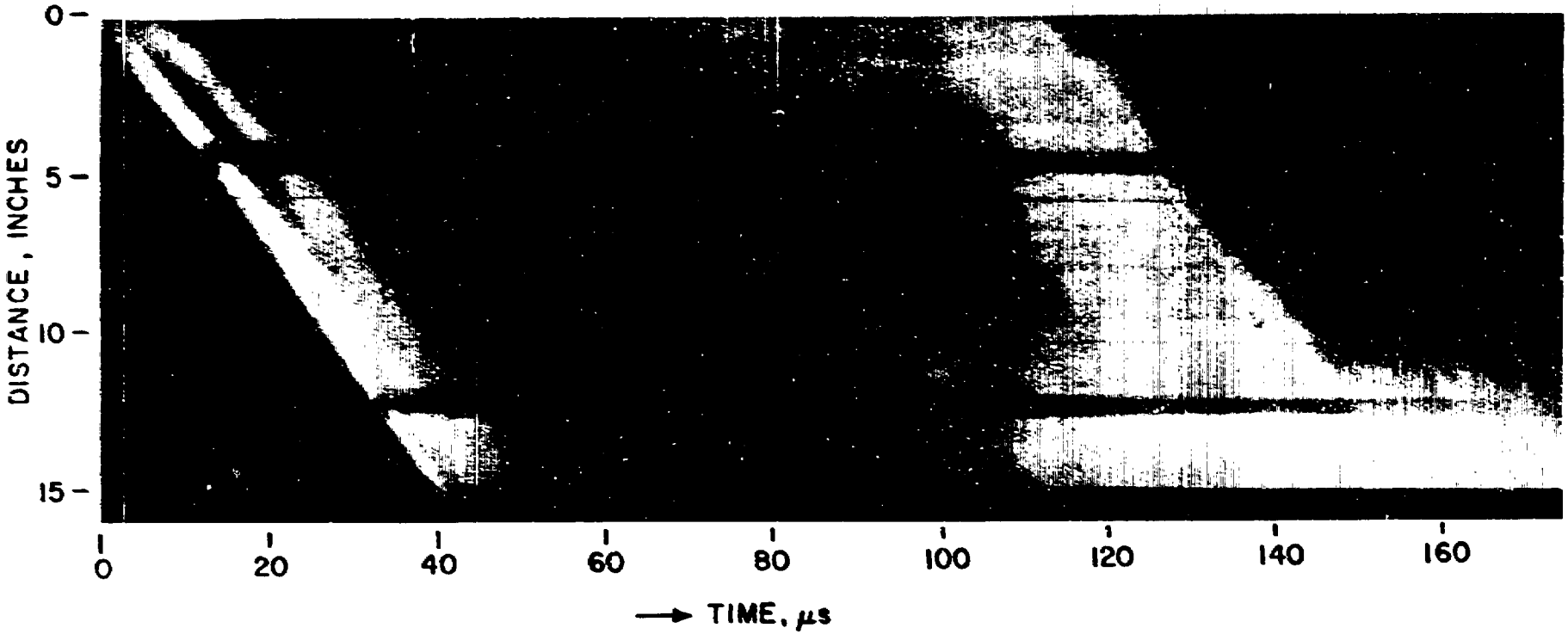

Fig. 5 A streak photograph of the flow in the accelerator. Curvature of the shock front, indicating acceleration of the gas can be observed. The streaks are due to gas particles of high luminosity.

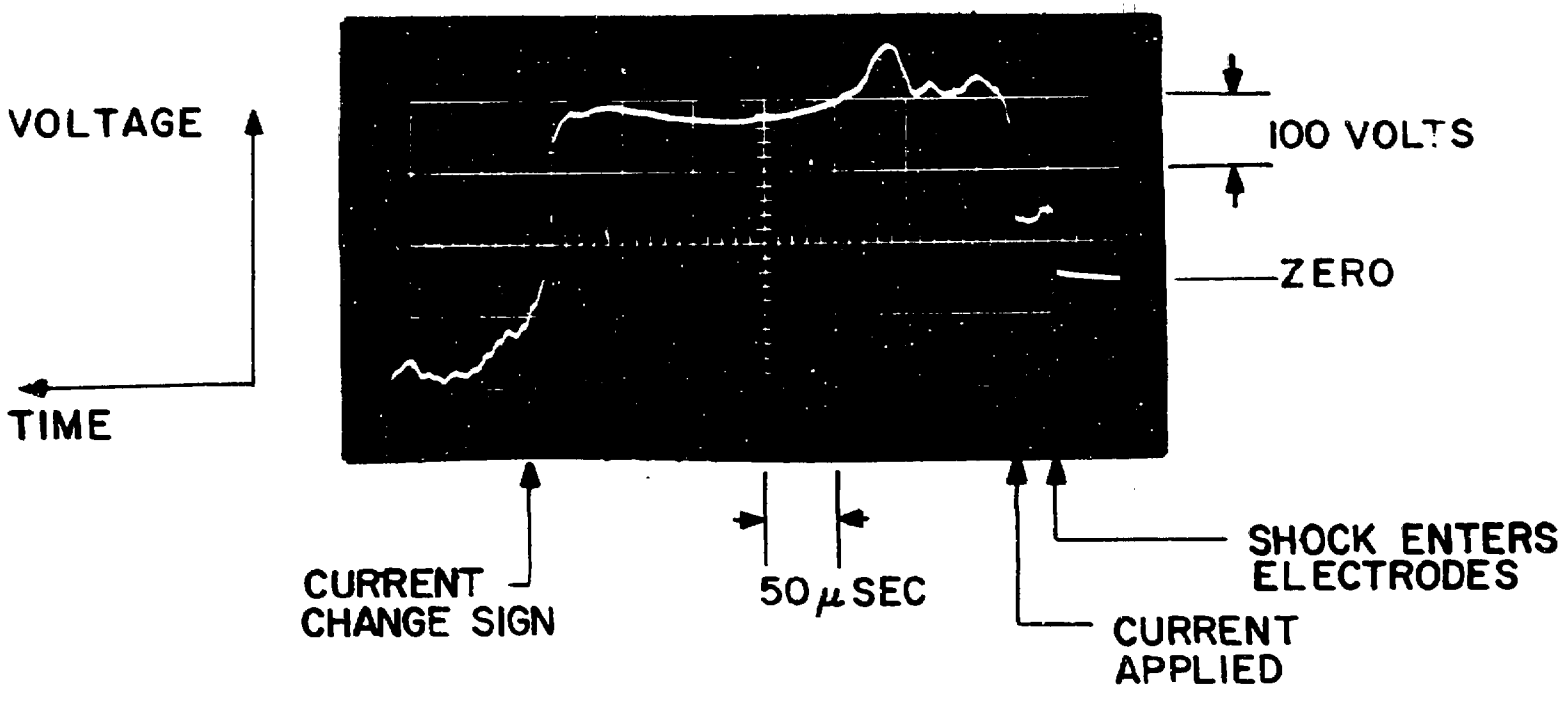

Fig. 6 The potential difference between the electrodes for a typical run. During the period after the shock entered the electrodes and before the current was applied, the accelerator acted as a flowmeter.

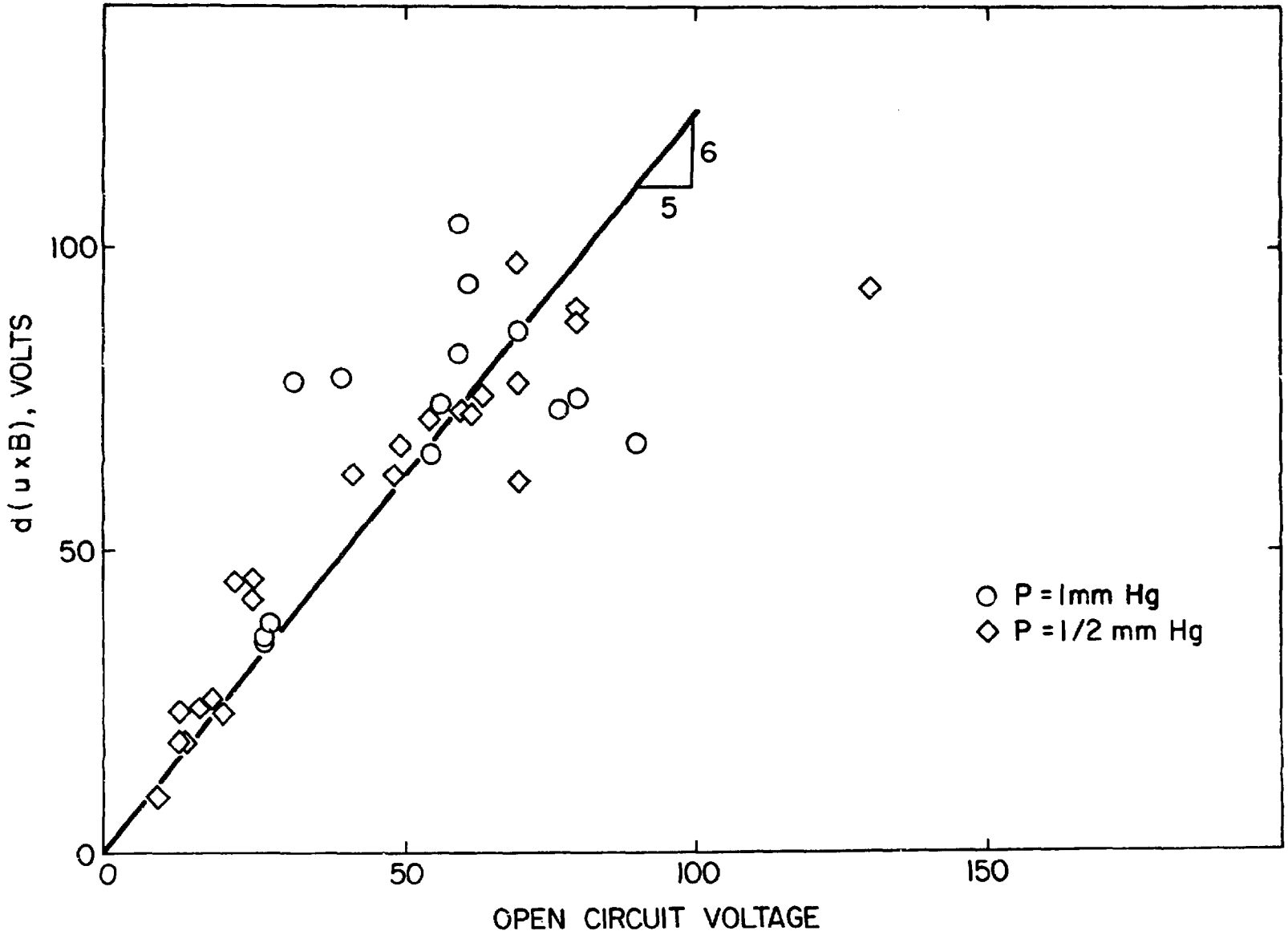

Fig. 7 Calibration of the accelerator as a flowmeter. The flow velocity used in computing the ordinate was calculated from the measured shock velocity.

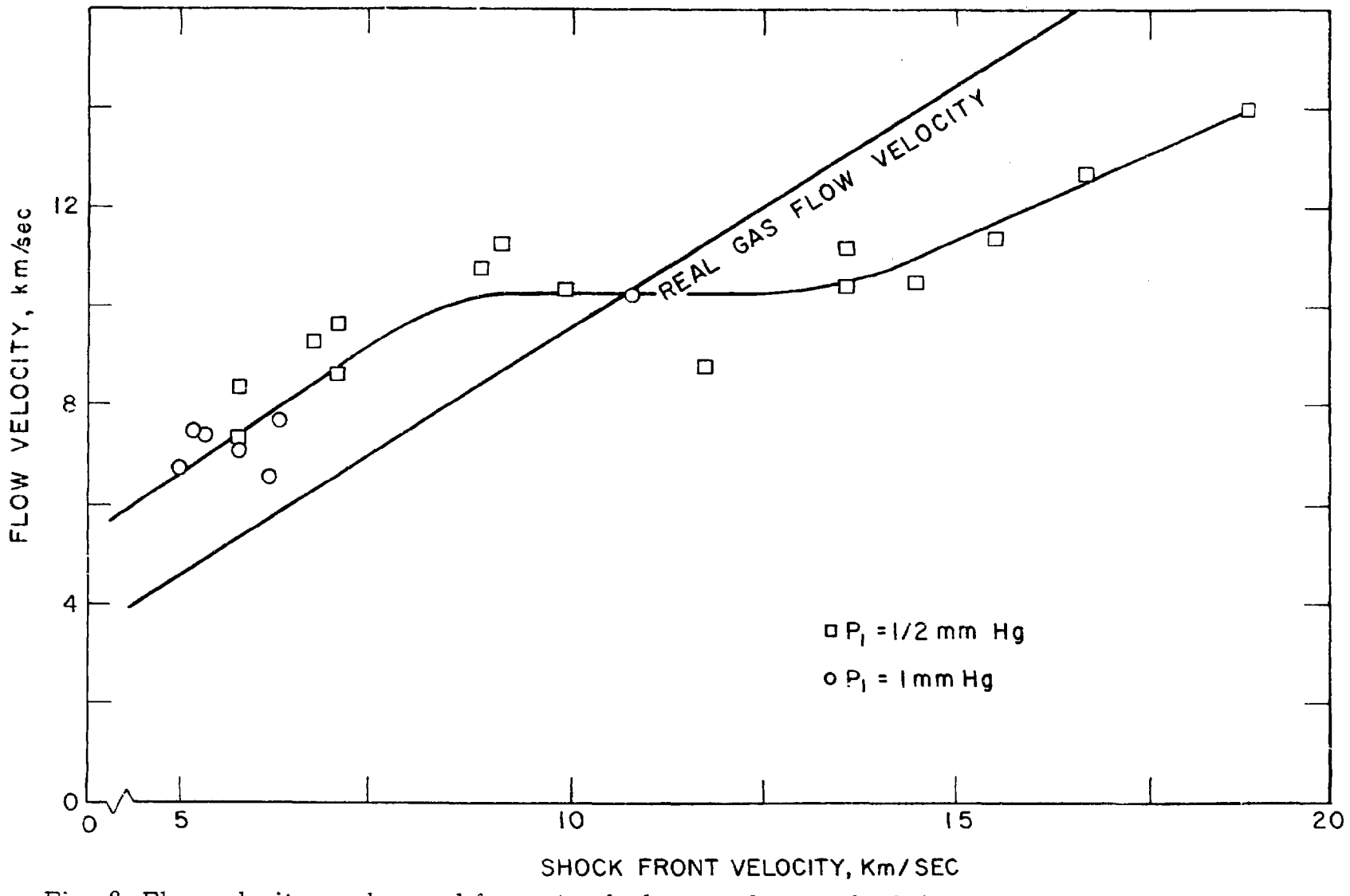

Fig. 8 Flow velocity as observed from streak photographs vs. shock front velocity. The line drawn was used to interpolate flow velocities for runs where streaks could not be distinguished, but in which the front velocity was measured. Straight line is the calculated particle velocity behind a shock whose velocity is given on the abscissa.

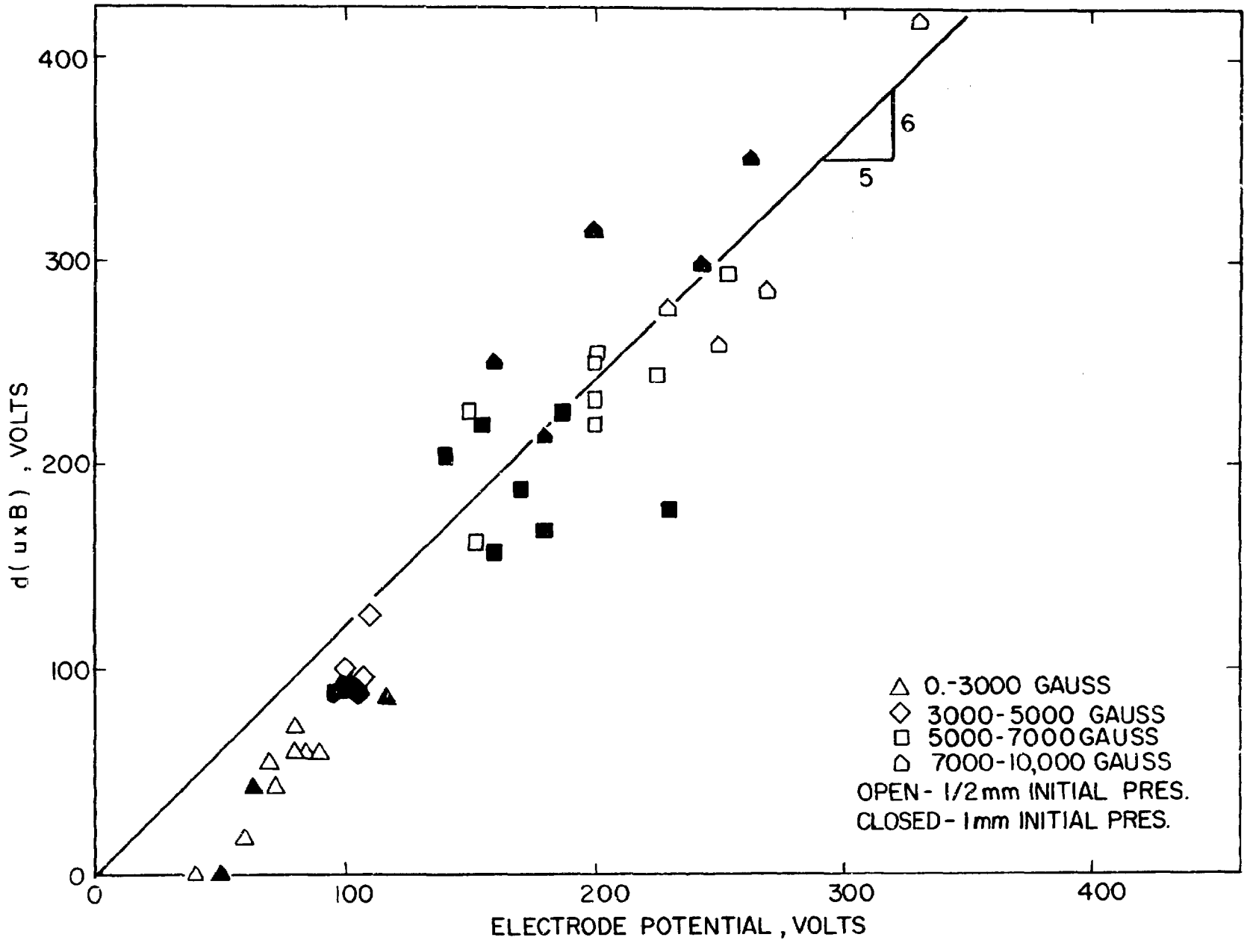

Fig. 9 The calculated induced voltage due to the accelerated gas in the magnetic field vs. the measured electrode potential showing the attainment of the E/B velocity.

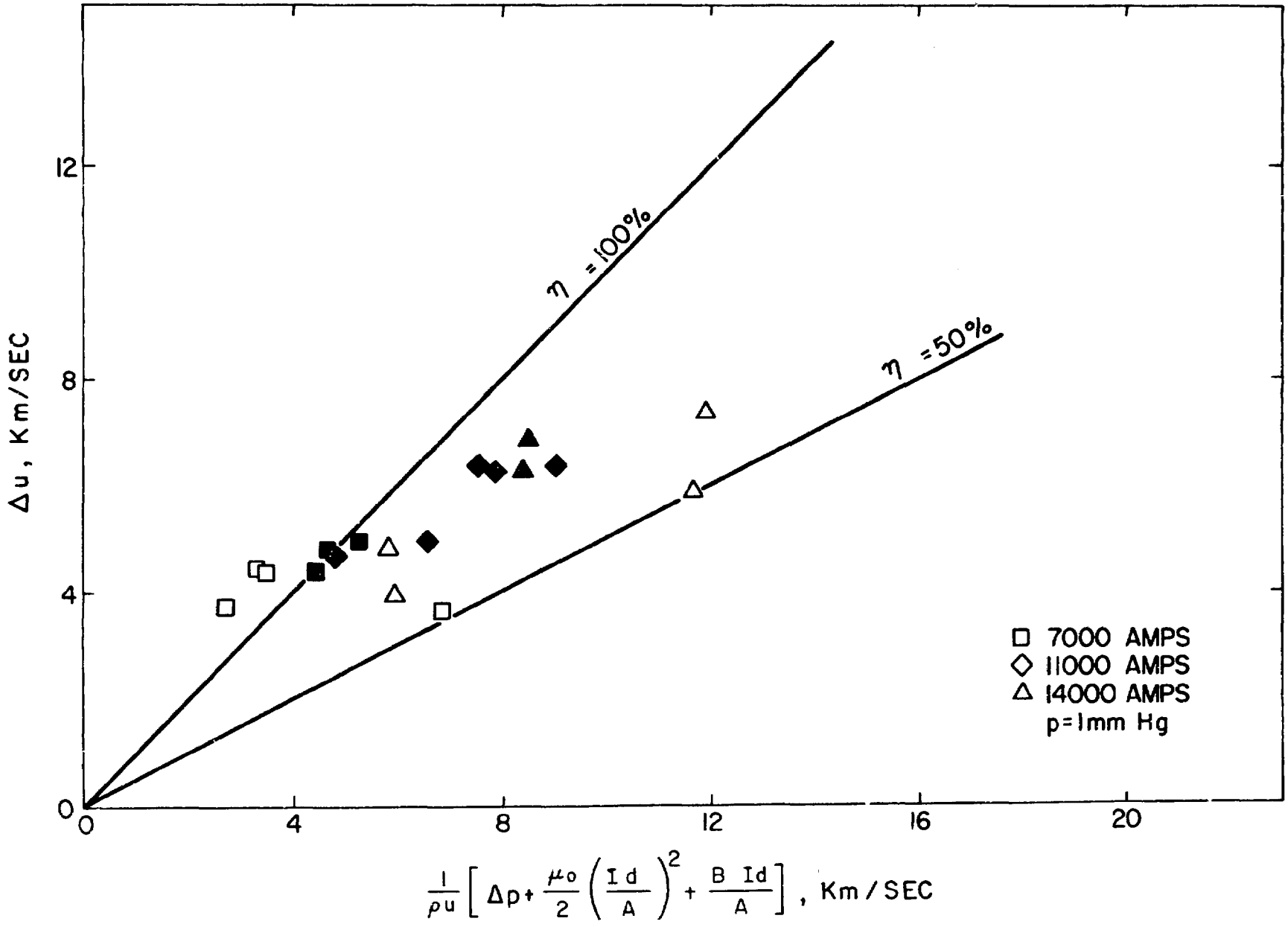

Fig. 10 Momentum balance for the accelerator at an initial pressure of 1 mm Hg at various applied currents. The closed figures are interpolated values for Δu from Fig. 8.

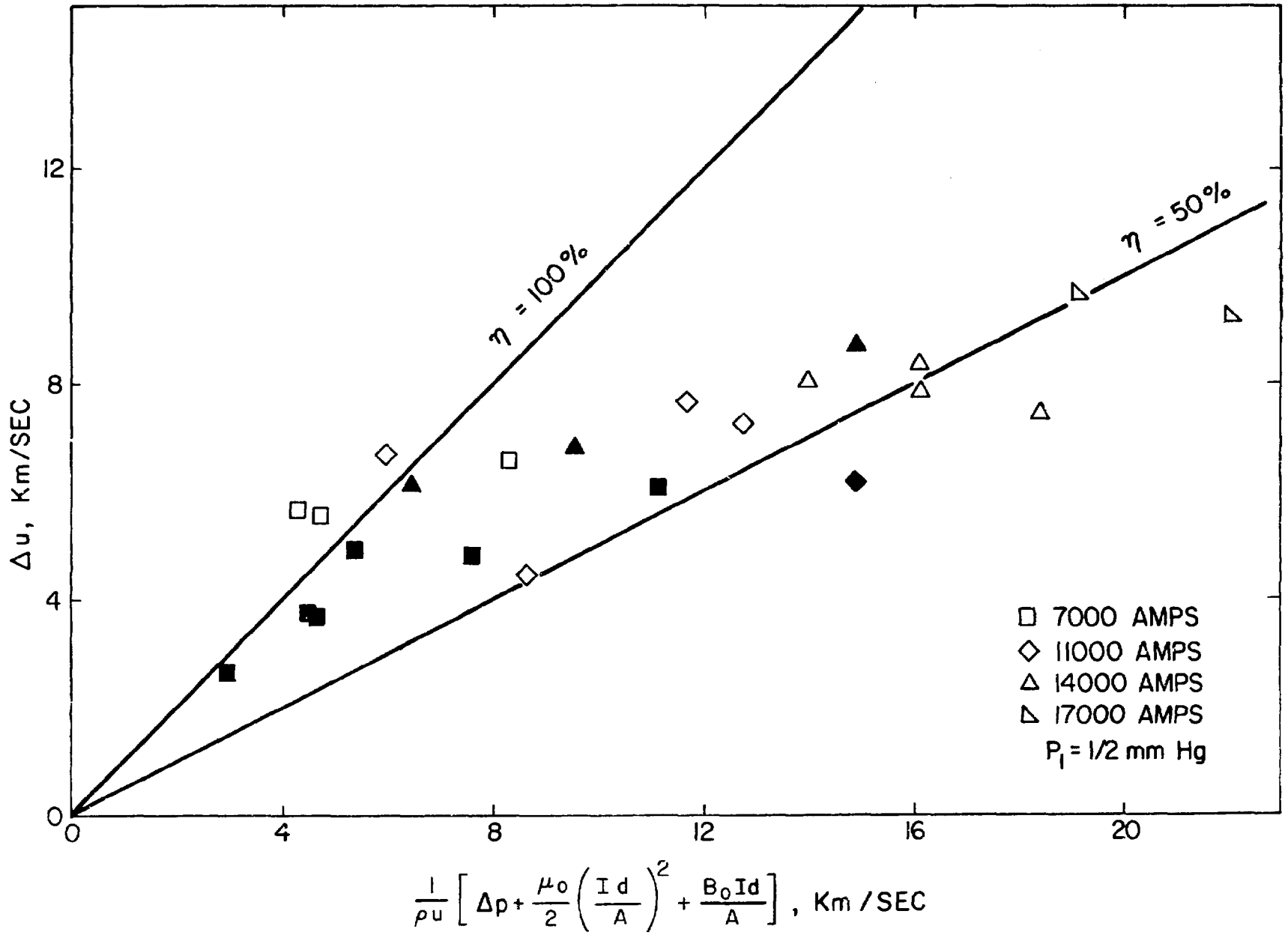

Fig. 11 Momentum balance for the accelerator at an initial pressure of 1/2 mm Hg at various applied currents. The closed figures are interpolated values for Δu from Fig. 8.

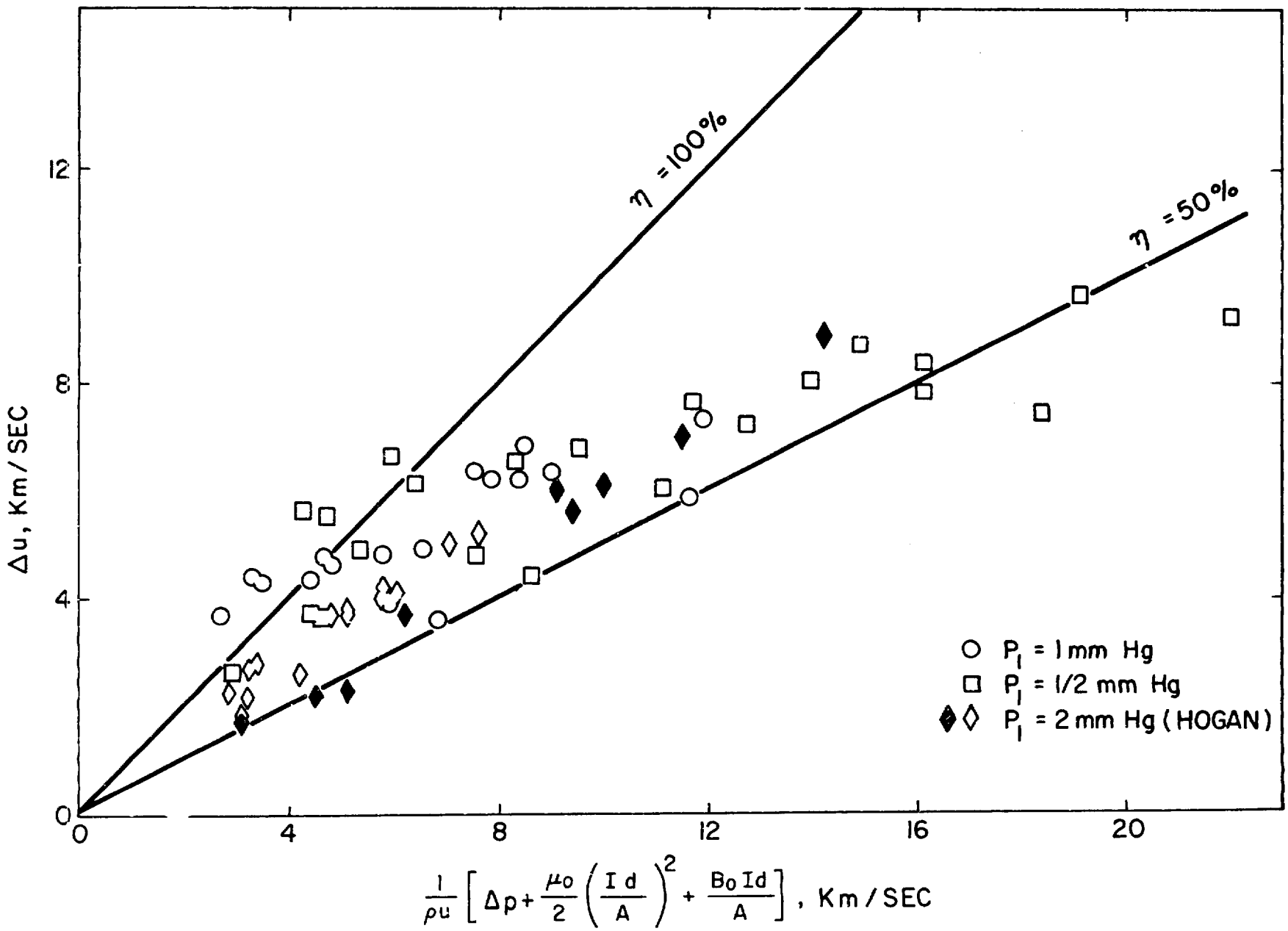

Fig. 12 Momentum balance for the accelerator for various initial pressures. Data at 2 mm was taken from Hogan[20]. The closed figures are for Hogan's long accelerator and the open figures from his short accelerator; both are taken from his Fig. 15.

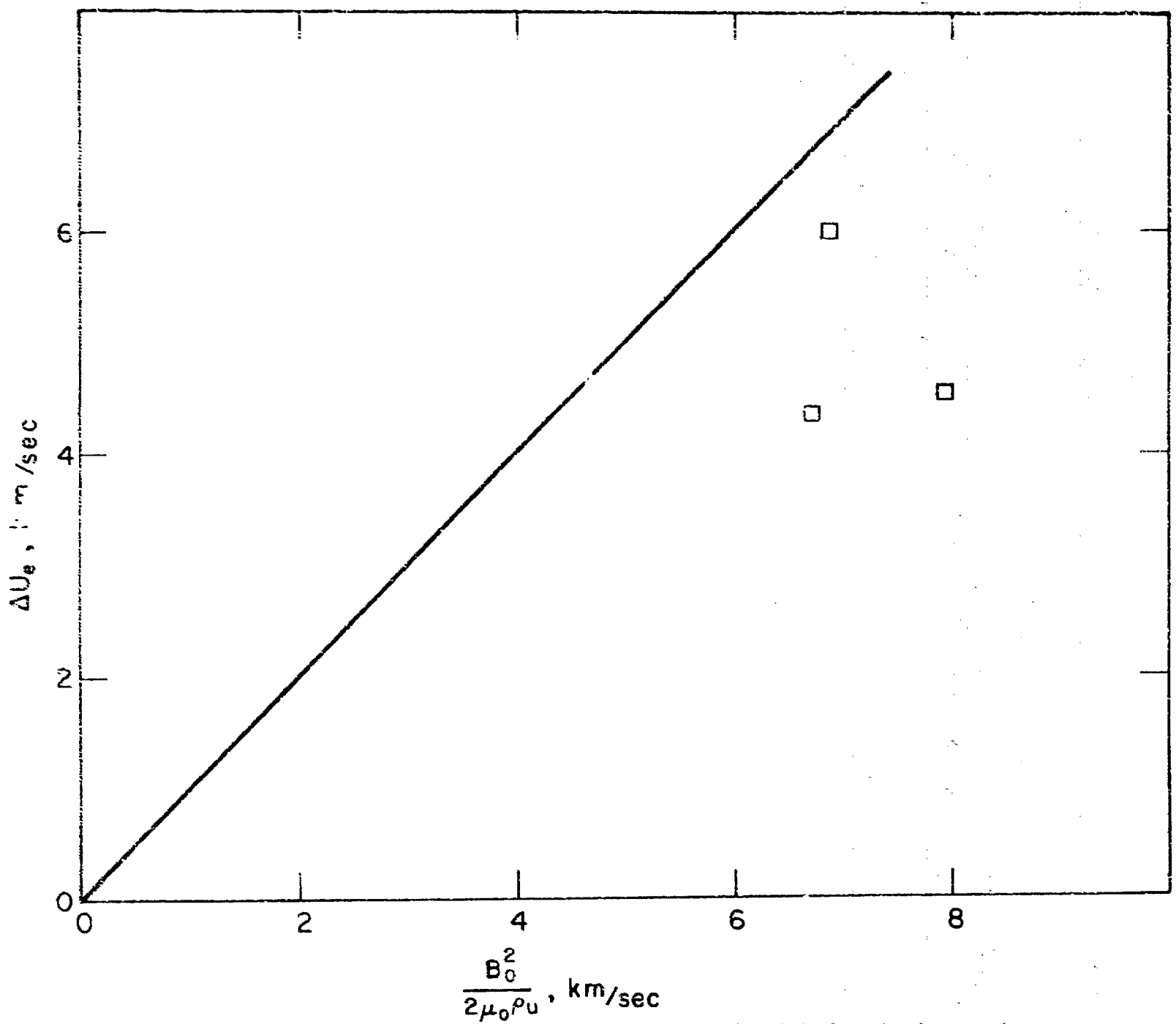

Fig. 13 The velocity decrease at the exit of the accelerator. Straight line is the maximum theoretical decrease.

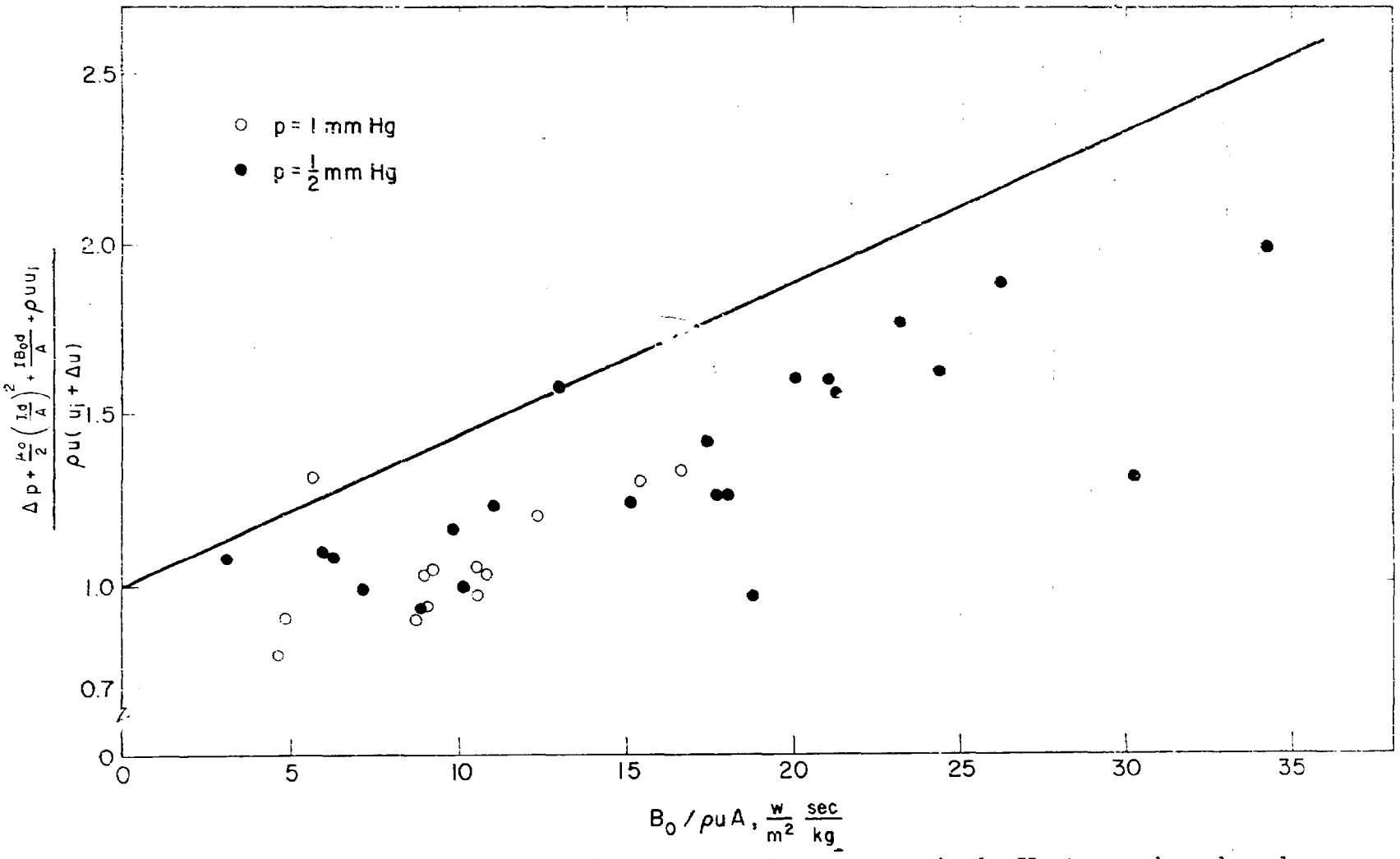

Fig. 14 Momentum balance for the accelerator assuming currents in the Hartmann boundary layer. The line drawn assumed losses predicted by an incompressible Hartmann profile assuming that the argon has transport properties equivalent to those of equilibrium argon at 1 atmosphere and 10,000°K.